

# Bifurcations and Chaos in Electrostatic Vibration Energy Harvesters

Elena Blokhina<sup>1</sup>, Dimitri Galayko<sup>2</sup>, Rhona Wade<sup>1</sup>, Philippe Basset<sup>3</sup> and Orla Feely<sup>1</sup>

<sup>1</sup> University College Dublin, Ireland

<sup>2</sup> Universite Pierre et Marie-Curie, France

<sup>3</sup> Université Paris-Est, ESYCOM, ESIEE Paris, France

**Abstract**—In this paper, we present an analysis of an electrostatic vibration harvester operating in the constant-charge mode. The goal of the study is to bound regions of control parameters where the system displays steady-state harmonic oscillations as required for practical use. We show how the system can be presented as a nonlinear oscillator and analysed employing the multiple scales method, Floquet theory and Lyapunov exponents. We determine the conditions for the onset of steady-state oscillations, the period doubling bifurcation and transition to chaos. This allows us to bound regions of control parameters where the system displays desired regular oscillations and, therefore, to identify maximal harvestable power for a particular architecture.

## I. INTRODUCTION

Electrostatic (capacitive) vibration energy harvesters (e-VEHs) convert kinetic energy of the environment into electrical energy using a capacitive transducer [1]. E-VEHs are particularly suitable for microscale implementation, and in recent years they have become the subject of a growing area of research [2]–[4]. The main issue of e-VEH design is the optimization of converted power for given environmental conditions and given limitations on the electrical and mechanical components. One of the limits of convertible power is set by the complexity and nonlinearity of the system, as demonstrated in [5]. In particular, desired harmonic oscillations are possible only for some set of system parameters. Otherwise, the system displays chaotic behaviour (non-harmonic modes) in which the conditioning electronics cannot operate properly. For these reasons, optimal design of a e-VEH requires a deep understanding of the overall system dynamics, including nonlinear effects.

The work [6] introduced an analytical tool for analysis of a e-VEH as the coupled system, while ref. [7] studies steady-state oscillations in the harvester applying a formal analytical approach. Building on these works, the aim of this paper is to extend the analysis of the e-VEH behaviour in order to identify the limit of regular harmonic operation of a e-VEH that employs a gap-closing transducer (one of the most widely used). We study bifurcations of the steady-state orbit and determine the condition for the period doubling bifurcation.

## II. STATEMENT OF THE PROBLEM

A simple electrostatic harvester consists of a high- $Q$  resonator, a variable capacitor (transducer)  $C_{tran}$ , and a conditioning circuit (Fig. 1). The displacement  $x$  of the mass-spring-damper system driven by the external oscillations and affected by the transducer force is described by

$$\ddot{x} + (b/m)\dot{x} + \omega_0^2 x = A_{ext} \cos(\omega_{ext}t + \vartheta_0) + f_t(x, \dot{x})/m \quad (1)$$

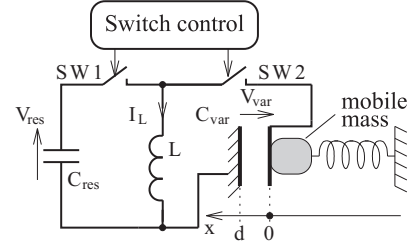


Fig. 1. Schematic view of an electrostatic vibration energy harvester.

where  $m$  is the mass of the resonator,  $b$  is the damping factor,  $\omega_0 = \sqrt{k/m}$  is the natural frequency,  $k$  is the spring constant,  $A_{ext}$  is the external acceleration amplitude,  $\omega_{ext}$  is the external frequency and  $\vartheta_0$  is the phase of the external force.  $f_t(x, \dot{x})$  is the force generated by the transducer. The detailed description of the conditioning circuit can be found in [4], [6].

Depending on the architecture of the conditioning circuit, at each cycle one quantity can be fixed on the transducer when  $C_{tran} = C_{max}$ : the charge  $Q_0$ , the energy  $W_0$ , or the voltage  $V_0$ . In this paper, we consider the most common case described in [4] where the energy  $W_0$  is fixed.

For a gap-closing transducer, the capacitance function is [5], [6]  $C_{tran} = C_0/(1 - x/d)$ , and the transducer force is

$$f_{t,2}(x, \dot{x}) = \begin{cases} \frac{W_0}{d(1-x_{max}/d)}, & \dot{x} \leq 0 \\ 0 & \dot{x} > 0 \end{cases} \quad (2)$$

Here  $d$  is the equilibrium gap and  $x_{max}$  is the maximal displacement.

In order to reduce the number of parameters and outline only essential ones, the following normalised variables are introduced: time  $\tau = \omega_0 t$ , dissipation  $\beta = b/(2m\omega_0)$ , normalised external frequency  $\Omega = \omega_{ext}/\omega_0 = 1 + \sigma$ ,  $y = x/d$ ,  $\alpha = A_{ext}/(d\omega_0^2)$  and  $\nu_0 = W_0/(d^2 m \omega_0^2)$ . Equation (1) is now written as

$$y'' + 2\beta y' + y = f_t(y, y') + \alpha \cos(\Omega\tau + \theta_0) \quad (3)$$

where the prime denotes the derivative with respect to dimensionless time  $\tau$  and the function  $f_t(y, y')$  is the normalised version of (2):

$$f_t(y, y') = \begin{cases} \frac{\nu_0}{(1-y_{max})}, & y' \leq 0 \\ 0 & y' > 0 \end{cases} \quad (4)$$

While the mass, the natural frequency and other parameters are fixed, the acceleration  $A_{ext}$  and the energy  $W_0$  (and their

dimensionless analogues  $\alpha$  and  $\nu_0$ ) may vary and affect the behaviour of the system. We will refer to them as the control parameters of the dynamical system. Typical parameters used in the numerical simulations of later sections are listed in Table I.

TABLE I  
PARAMETERS OF THE SYSTEM

m	$200 \cdot 10^{-6}$ kg
b	$\sqrt{2} \cdot 10^{-3}$ Nsm $^{-1}$
k	300 Nm $^{-1}$
d	$20 \cdot 10^{-6}$ m
S	$10 \cdot 10^{-4}$ m $^2$
$W_0$	$0.5 - 3 \cdot 10^{-8}$ J
$A_{ext}$	$1 - 10$ ms $^{-2}$

### III. STEADY-STATE OSCILLATIONS

In this section we very briefly discuss steady-state behaviour. Substantial results that we have recently obtained for the system with two configurations of the transducer, area overlap [8] and hyperbolic [5], are reported in [7]. We analyse the steady-state behaviour by employing the multiple scales method (MSM) [9], a type of perturbation technique that is often applied for the analysis of weakly nonlinear oscillators of various types, both autonomous and under external excitation. The solution obtained from the MSM has the form

$$y_0(\tau) = y_{av,0} + a_0 \cos((1 + \sigma)\tau + \theta_0 - \psi_0) \quad (5)$$

where  $a_0$ ,  $y_{av,0}$  and  $\psi_0$  are the steady-state amplitude, average displacement (constant shift) and phase of oscillations (the index '0' emphasizes that this is a steady-state solution). The amplitude  $a_0$  and the phase  $\psi_0$  are found from the equations:

$$\frac{\alpha}{2} \sin \psi_0 = \beta a_0 + \frac{b_1(y_{m,0})}{2}, \quad \frac{\alpha}{2} \cos \psi_0 = -a_0 \sigma - \frac{a_1(y_{m,0})}{2}$$

$$\frac{\alpha^2}{4} = \left( \beta a_0 + \frac{b_1(y_{m,0})}{2} \right)^2 + \left( a_0 \sigma + \frac{a_1(y_{m,0})}{2} \right)^2 \quad (6)$$

where  $y_{m,0}$  denotes the maximal displacement  $y_{m,0} = y_{av,0} + a_0$ . The transducer force is a periodic function since the solution (5) is a harmonic oscillation. Therefore, we have used the Fourier series for  $f_t$

$$f_t(\tau) = f_0 + a_1 \cos \theta(\tau) + b_1 \sin \theta(\tau)$$

where  $\theta(\tau) = (1 + \sigma)\tau + \theta_0 - \psi_0$  and the functions  $f_0$ ,  $a_1$  and  $b_1$  are the standard coefficients of the Fourier series but dependent on the amplitude  $a_0$  and the average displacement  $y_{av,0}$ . Note that due to the zero harmonic in the Fourier series, the oscillation (5) has this constant shift  $y_{av,0} = f_0$ .

The orbit given by (5)-(6) is stable if the following conditions are fulfilled:

$$2\beta + \frac{b'_1}{2} + \frac{b_1}{2a_0} > 0$$

$$\left( \beta + \frac{b'_1}{2} \right) \left( \beta + \frac{b_1}{2a_0} \right) + \left( \sigma + \frac{a'_1}{2} \right) \left( \sigma + \frac{a_1}{2a_0} \right) > 0 \quad (7)$$

If the above conditions are not fulfilled, the orbit that is defined by these  $a_0$ ,  $y_{av,0}$  and  $\psi_0$  is unstable, or a saddle orbit. The above stability condition is necessary, but not sufficient.

For the gap closing transducer, the coefficients are

$$f_0 = \frac{\nu_0}{2(1 - y_m)}, \quad a_1 = 0, \quad b_1 = \frac{2\nu_0}{\pi(1 - y_m)} \quad (8)$$

### IV. NONLINEAR BEHAVIOUR AND BIFURCATIONS

#### A. Motivation for Further Analysis.

In the previous section we noted the necessary condition for stability following ref. [7]. However, it is known that for nonlinear oscillators increase in the amplitude of the external force or other parameters typically leads to bifurcations of previously stable orbits and, eventually, to irregular, chaotic behaviour [10]. We have carried out a series of numerical simulations of the system shown in Fig. 1 using a VHDL-AMS model [11]. A typical result is shown in Fig. 2. A slowly growing ramp of the acceleration envelope  $A_{ext}$  versus time is depicted in Fig. 2a. At the same time, we trace the displacement of the resonator versus time in Fig. 2b. Since the ramp changes very slowly, we consider this process as quasi-static and therefore we observe the evolution of the steady-state behaviour of the e-VEH at a variation of  $A_{ext}$ . This plot can be seen as an analogue of a bifurcation diagram.

According to Fig. 2, there are the following qualitative changes (bifurcations) in the system behaviour with a change of the parameter  $A_{ext}$ : (i) appearance of steady-state harmonic oscillations (fragment 1 in the figure); (ii) period doubling bifurcation (fragment 2, see Fig. 3a) and (iii) transition to chaos (fragment 3, see Fig. 3b). Two closed orbits and a portion of a chaotic trajectory at fixed  $A_{ext}$  and  $W_0$  that illustrates the above bifurcations are shown in Fig. 4.

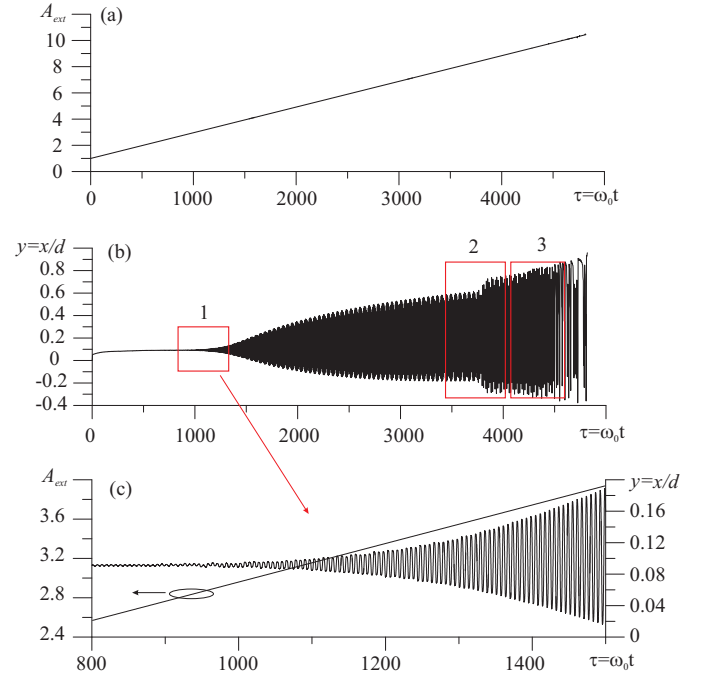


Fig. 2. (a) A slowly growing ramp of the envelope of the external oscillations  $A_{ext}$  and (b) the corresponding displacement of the harvester as functions of normalised time. Three fragments of principally different behaviour of the system are marked. Magnified fragment 1 demonstrating the onset of steady-state oscillations is shown in subfigure (c). The two other magnified fragments are shown in Fig. 3.  $W_0 = 20$  nJ.

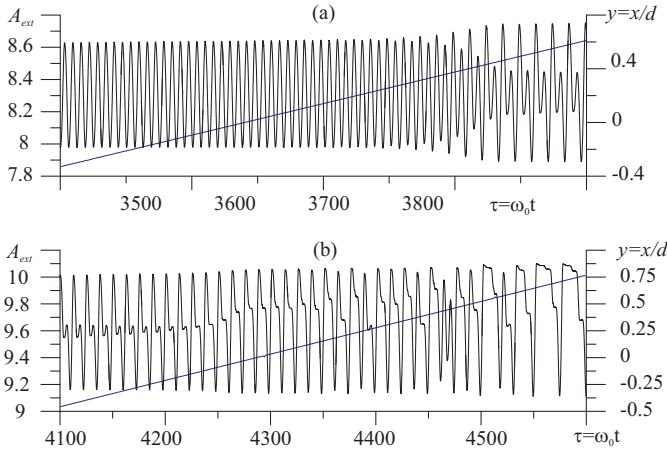


Fig. 3. A slowly growing ramp of  $A_{ext}$  the envelope of the external oscillations (the blue line, refer to the axis on the left) and the corresponding displacement of the harvester (the black line, refer to the axis on the right) as functions of normalised time. Figure (a) is a magnified fragment 2 from Fig. 2 and shows the doubling bifurcation. Figure (b) is a magnified fragment 3 and shows transition to chaos.  $W_0 = 20 \text{ nJ}$ .

The analysis performed with the MSM allows us to determine the onset of steady-state oscillations [5], [7]. The necessary condition for the onset is obtained by letting  $a_0 = 0$  in (6):

$$\alpha^{min} = 2\nu_0/\pi \quad \text{or} \quad \nu_0^{max} = \pi\alpha/2 \quad (9)$$

or in the dimensional values,

$$A_{ext}^{min} = 2W_0/(\pi md) \quad \text{or} \quad W_0^{max} = \pi md A_{ext}/2 \quad (10)$$

This means that in order to put the system in oscillations at  $A_{ext} = 3 \text{ m/s}^2$ , the parameter  $W_0$  must be selected less than  $W_0^{max} = 18.9 \text{ nJ}$ .

### B. Equation for Small Perturbations and Floquet Multipliers.

Now we introduce a small deviation  $\zeta$  from the steady-state solution  $y_0$  and assume that solution of (3) is  $y(\tau) = y_0(\tau) + \zeta(\tau)$ . The perturbation of the displacement  $\zeta$  will cause a perturbation  $y_{m,\zeta}$  of the maximal displacement about the steady-state value state  $y_{m,0}$ :  $y_m = y_{m,0} + y_{m,\zeta}$ . Since this perturbation is small, the functions  $f_0(y_m)$  and  $b_1(y_m)$  can be represented as

$$f_0 = f_0(y_{m,0}) + f_0'(y_{m,0})y_{m,\zeta}, \quad b_1 = b_1(y_{m,0}) + b_1'(y_{m,0})y_{m,\zeta}$$

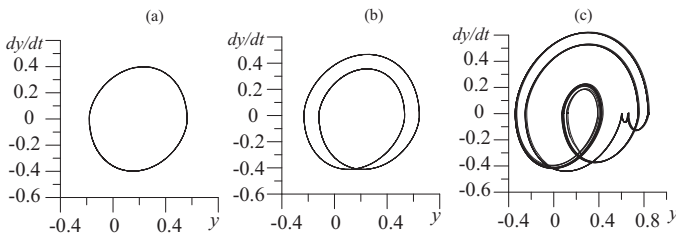


Fig. 4. Trajectories in the state space: (a) a closed orbit that corresponds to harmonic steady-state oscillations (5) at  $A_{ext} = 7.5 \text{ m/s}^2$  (b) a closed orbit at  $A_{ext} = 8.5 \text{ m/s}^2$  after the period doubling bifurcation and (c) a chaotic attractor at  $A_{ext} = 9.5 \text{ m/s}^2$ .  $W_0 = 20 \text{ nJ}$ .

and we obtain the equation

$$\zeta'' + 2\beta\zeta' + \zeta = f_0'(y_{m,0})y_{m,\zeta} + b_1'(y_{m,0})y_{m,\zeta} \sin(\Omega\tau + \theta_0 - \psi_0) \quad (11)$$

that generally describes the evolution of small deviations from the steady-state orbit. Note that the prime for the functions  $f_0$  and  $b_1$  is taken with respect to their argument, i.e.  $y_m$ . This equation contains the variable  $y_{m,\zeta}$  which is undefined analytically in the most general case. To address this issue, we can choose to launch the initial deviation at the moment when  $y' = 0$ , i.e. then,  $y_{m,\zeta}(0) = \zeta(0)$ , and we will use  $\zeta$  instead of  $y_{m,\zeta}$ . This ‘trick’ significantly simplifies the analysis.

$$\zeta'' + 2\beta\zeta' + \zeta(1 - f_0'(y_{m,0}) - b_1'(y_{m,0}) \sin(\Omega\tau + \theta_0 - \psi_0)) = 0 \quad (12)$$

The latter can be reduced to a well-known parametric equation, the Mathieu Equation

$$\xi'' + (\delta + 2\varepsilon \cos 2t)\xi = 0 \quad (13)$$

by introducing the variable transformations:

$$\zeta = \exp(-\beta t)\xi, \quad \tau = 2t/\Omega + \tau_0, \quad \tau_0 = (\psi_0 - \theta_0 - \pi/2)/\Omega$$

$$\delta = \frac{4}{\Omega^2}(1 - \beta^2 - f_0'(y_{m,0})), \quad 2\varepsilon = \frac{4}{\Omega^2}b_1'(y_{m,0})$$

For equation (13), it is known that for certain  $\delta$  and  $\varepsilon$ , there exist areas of so-called ‘parametric instability’ when the solution of (13)  $\xi = 0$  is unstable [9]. Returning to the original system, this means that the small deviations  $\zeta$  of the steady-state  $y_0$  will start increasing instead of decaying. The areas of parametric instability for the Mathieu equation are found in the latter reference. Thus, we can determine stability of the orbit simply by checking whether  $\delta$  and  $\varepsilon$  defined for equation (12) lie in one of parametric instability areas.

However, a more complete analysis of parametric equations can be obtained by employing Floquet theory [10] that not only provides us with bifurcation values of parameters but also indicates what type of bifurcation is undergone by the original orbit. For this purpose, one constructs a matrix equation based on the equation for small perturbations (12):

$$\begin{pmatrix} \zeta_1' & \zeta_2' \\ \eta_1' & \eta_2' \end{pmatrix} = \begin{pmatrix} 0 & 1 \\ K(\tau) & -2\beta \end{pmatrix} \begin{pmatrix} \zeta_1 & \zeta_2 \\ \eta_1 & \eta_2 \end{pmatrix} \quad (14)$$

where the prime denotes the derivative with respect to time  $\tau$ ,  $\eta = d\zeta/d\tau$  and the time dependent coefficient  $K(\tau)$  is  $K(\tau) = [-1 + f_0'(y_{m,0}) + b_1'(y_{m,0}) \sin(\Omega\tau + \theta_0 - \psi_0)]$ . The latter allows one to find a set of fundamental solutions (two fundamental solutions in our particular case). Denoting  $\mathbf{Z} = \begin{pmatrix} \zeta_1 & \zeta_2 \\ \eta_1 & \eta_2 \end{pmatrix}$ , we assume initial conditions for the set (14) in the form of the identity matrix  $\mathbf{Z}(0) = \mathbf{I}$ . Solving (14) on one period  $T = 2\pi/\Omega$  we obtain  $\mathbf{M} = \mathbf{Z}(T)$ , the monodromy matrix. The eigenvalues of the monodromy matrix  $\mathbf{M}$ , the Floquet multipliers  $\mu_k$ , indicate stability of the orbit. The orbit is asymptotically stable if there are no eigenvalues outside the unit circle. If at a variation of control parameter a Floquet multiplier leaves the unit circle through  $-1$ , the original fixed point or orbits undergoes a doubling bifurcation; if through  $+1$ , a transcritical, symmetry-breaking or cyclic-fold bifurcation, and, finally, if two complex conjugate multipliers

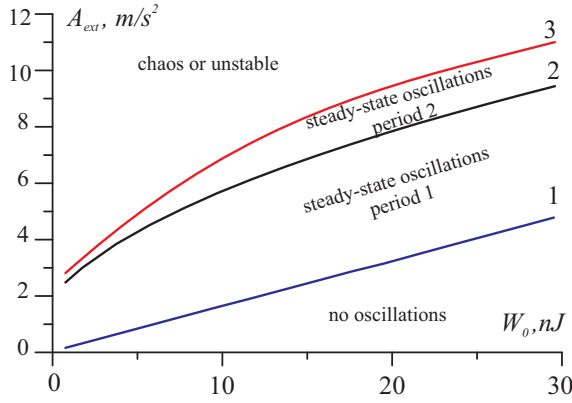


Fig. 5. Plane of parameter  $(W_0, A_{ext})$  where the different areas correspond to different regimes displayed by the system. Line 1 is the onset of steady-state oscillations, line 2 is the doubling bifurcation and line 3 is transition to chaos.

leave the circle, a Hopf bifurcation takes place in the system. Therefore, if solving (14) we calculate the Floquet multipliers, we can also define the type of a bifurcation.

### C. Lyapunov Exponents.

The Lyapunov exponents or characteristic exponents are associated with a trajectory and essentially measure the average rates of expansion and contraction of trajectories surrounding it [10]. They are asymptotic quantities, defined locally in state space, and describe the exponential rate at which a perturbation to a trajectory of a system grows or decays with time at a certain location in the state space. The existence of at least one positive Lyapunov exponent of an attractor is a criterion for chaos.

Formal mathematical definition of the largest Lyapunov exponent can be given as follows. Assume that there exists a steady state trajectory or a fixed point  $\mathbf{x}_0(t)$  in the state space. Now let us trace a perturbed trajectory  $\mathbf{x}(t)$  starting at  $t = 0$  from a small  $\delta$ -neighbourhood of  $\mathbf{x}(0)$ . The largest Lyapunov exponent is given by the expression:

$$\Lambda_1 = \lim_{t \rightarrow \infty} \frac{1}{t} \log \frac{\|\mathbf{x}(t) - \mathbf{x}_0(t)\|}{\|\mathbf{x}(0) - \mathbf{x}_0(0)\|} \quad (15)$$

This formula can be implemented in numerical simulations of the original nonlinear system (3) by solving two sets of this equation with a small variation in initial conditions. If  $\Lambda_1$  becomes positive at a variation of a control parameter, we consider that the regime becomes chaotic.

### D. Summary of the results: plane of control parameters.

Now we apply all the discussed techniques to plot a plane of parameters  $(W_0, A_{ext})$  with the main bifurcation lines depicted in it. An example of such plane is shown in Fig. 5. Line 1 (blue) shows the conditions (10) required to start steady-state harmonic oscillations in the resonator. Below this line one observes irregular small scale displacements of the resonator with many maxima detected in one period while above this line lies the area of steady-state oscillation. An illustration of such transition is shown in Fig. 2c obtained through VHDL-AMS modelling.

Line 2 (black) shows the doubling bifurcation and bounds the area of steady-state oscillations with period 2. The line was obtained by solving numerically the set of fundamental solutions (14) which yielded the monodromy matrix of the system. We trace when and how one of the Floquet multipliers leaves the unit circle. We have found out that the multipliers cross it through  $-1$  (therefore, it is a doubling bifurcation) and determined the bifurcation values of the parameters. This agrees with the modelling shown in Fig. 3a that clearly illustrate the period doubling of the original orbit. Note that resulting oscillations are stable as well.

Finally, line 3 indicates when the largest Lyapunov exponent becomes positive and the system displays chaotic oscillations. This line agrees with the modelling shown in Fig. 3b. It is very interesting that the system displays only one doubling bifurcation and therefore the transition to chaos is not through the Feigenbaum scenario but rather through intermittency.

## V. CONCLUSIONS

This study analysed an e-VEH as a nonlinear oscillator, focusing in particular on the limits of regular behaviour. The analysis presented here quantifies the phenomena observed previously in the behavioural model [5] and provides necessary and sufficient conditions for a regular harmonic mode of the e-VEH. This provides designers of e-VEHs with a powerful tool allowing them to understand fundamental limits of the system at early stages of design. All analytical discoveries are verified by simulations of the behavioral model carried out with VHDL-AMS.

## REFERENCES

- [1] P. Mitcheson, E. Yeatman, G. Rao, A. Holmes, and T. Green, "Energy harvesting from human and machine motion for wireless electronic devices," *Proceedings of the IEEE*, vol. 96, no. 9, pp. 1457–1486, 2008.
- [2] G. Despesse, T. Jager, J.J.Chailout, J. M. Lger, A. Vassilev, S. Basrour, and B. Charlot, "Fabrication and characterization of high damping electrostatic micro devices for vibration energy scavenging," in *Proceeding of DTIP of MEMS & MOEMS conference*, 2005.
- [3] P. Basset, D. Galayko, A. Paracha, F. M. A. Dudka, and T. Bourouina, "A batch-fabricated and electret-free silicon electrostatic vibration energy harvester," *Journal of Micromechanics and Microengineering*, vol. 19, p. 115025, 2009.
- [4] S. Meninger, J. Mur-Miranda, R. Amirtharajah, A. Chandrakasan, and J. Lang, "Vibration-to-electric energy conversion," *Very Large Scale Integration (VLSI) Systems, IEEE Transactions on*, vol. 9, no. 1, pp. 64–76, 2001.
- [5] D. Galayko, R. Guillemet, A. Dudka, and P. Basset, "Comprehensive dynamic and stability analysis of electrostatic vibration energy harvester (E-VEH)," in *2011 International Conference on Solid-State Sensors, Actuators and Microsystems (TRANSDUCERS)*, 2011, pp. 2382–2385.
- [6] D. Galayko and P. Basset, "A general analytical tool for the design of vibration energy harvesters (VEHs) based on the mechanical impedance concept," *IEEE Trans. Circuits Syst. I*, no. 99, pp. 299–311, 2011.
- [7] E. Blokhina, D. Galayko, P. Basset, and O. Feely, "Steady-state oscillations in electrostatic vibration energy harvesters," *IEEE Trans. Circuits Syst. II*, 2011 (submitted).
- [8] W. Tang, T. Nguyen, M. Judy, and R. Howe, "Electrostatic-comb drive of lateral polysilicon resonators," *Sensors and Actuators A: Physical*, vol. 21, no. 1-3, pp. 328–331, 1990.
- [9] A. Nayfeh, *Introduction to perturbation techniques*. Wiley, 1993.
- [10] A. Nayfeh and B. Balachandran, *Applied nonlinear dynamics*. Wiley-VCH, 2004.
- [11] D. Galayko, R. Pizarro, P. Basset, and A. Paracha, "AMS modeling of controlled switch for design optimization of capacitive vibration energy harvester," in *IEEE International Workshop on Behavioral Modeling and Simulation*. IEEE, 2007, pp. 115–120.